

## An instrumented glove for monitoring hand function

A. Mohan, G. Tharion, R. K. Kumar, and S. R. Devasahayam

Citation: [Review of Scientific Instruments](#) **89**, 105001 (2018); doi: 10.1063/1.5038601

View online: <https://doi.org/10.1063/1.5038601>

View Table of Contents: <http://aip.scitation.org/toc/rsi/89/10>

Published by the [American Institute of Physics](#)

---

### Articles you may be interested in

[Passive bistatic radar using digital video broadcasting–terrestrial receivers as general-purpose software-defined radio receivers](#)

[Review of Scientific Instruments](#) **89**, 104701 (2018); 10.1063/1.5048132

[Tomographic analysis of tangential viewing cameras \(invited\)](#)

[Review of Scientific Instruments](#) **89**, 10K110 (2018); 10.1063/1.5038586

[Note: Biochemical samples centrifuged in-flight on drones](#)

[Review of Scientific Instruments](#) **89**, 106102 (2018); 10.1063/1.5031039

---



**PFEIFFER VACUUM**

**VACUUM SOLUTIONS FROM A SINGLE SOURCE**

Pfeiffer Vacuum stands for innovative and custom vacuum solutions worldwide, technological perfection, competent advice and reliable service.

[Learn more!](#)

## An instrumented glove for monitoring hand function

A. Mohan,<sup>1,2,a)</sup> G. Tharion,<sup>3,b)</sup> R. K. Kumar,<sup>4,c)</sup> and S. R. Devasahayam<sup>1,d)</sup>

<sup>1</sup>Department of Bioengineering, Christian Medical College Vellore, Vellore, India

<sup>2</sup>Department of Biotechnology, Indian Institute of Technology Madras, Chennai, India

<sup>3</sup>Department of Physical Medicine and Rehabilitation, Christian Medical College Vellore, Vellore, India

<sup>4</sup>Department of Engineering Design, Indian Institute of Technology Madras, Chennai, India

(Received 4 May 2018; accepted 14 September 2018; published online 3 October 2018)

The measurement of hand kinematics is important for the assessment and rehabilitation of the paralysed hand. The traditional method of hand function assessment uses a mechanical or electronic goniometer placed across the joint of interest to measure the range of joint movement. Mechanical goniometers are imprecise and lack the ability to provide a dynamic measurement; electronic goniometers are expensive and cumbersome to use during therapy. An alternative to the goniometric based assessment is to use inertial motion sensors to monitor the hand movement—these can be incorporated in a glove. In this paper, we present the design of an instrumented glove equipped with Magnetic, Angular Rate and Gravity (MARG) sensors for the objective evaluation of hand function. The instrumented glove presented in this paper is designed to assess the range of movement of the hand and also monitor the hand function during the course of hand rehabilitation. Static and dynamic calibrations were performed for the Euler angles calculated from the MARG sensors. The results are also presented for physiological flexion/extension of the wrist (relative roll), flexion/extension of elbow (relative pitch), and internal rotation/external rotation (relative yaw). The static calibration results gave mean absolute errors of 4.1° for roll, 4.0° for pitch, and 4.6° for yaw. From the dynamic calibration, the speed of response to a step change gave a convergence time of 0.4 s; sinusoidally oscillating movement gave good tracking at 0.2 Hz but exhibits overshoot errors at higher frequencies which were tested to be 1 Hz. We present the results of the calibration of the instrumented glove (one sensor pair measuring one joint angle) measuring anatomical joint angles—mean absolute errors during static calibration: 6.3° for a relative roll (wrist flexion/extension), 5.0° for relative pitch (elbow flexion/extension), and 4.5° for relative yaw (shoulder internal rotation/external rotation). The experimental results from the instrumented glove are promising, and it can be used as an alternative to the traditional goniometer based hand function assessments. *Published by AIP Publishing.* <https://doi.org/10.1063/1.5038601>

### I. INTRODUCTION

Objective assessment of the motor function of the hand is performed primarily using goniometers (electronic or mechanical) during the course of hand recovery from a neurological impairment. The therapist positions the goniometer on both sides of the joint of interest to measure the range of movement. The results are recorded manually. Goniometer based assessment of the motor function is simple and can be readily employed in clinical settings, but is prone to be inaccurate and time consuming. Also, certain clinically relevant features such as speed of movement and quality of movement (presence or absence of tremor) are paid little or no attention due to the lack of measurement devices or because of the time needed for the assessment.

An alternative to the traditional method of hand assessment using a goniometer is the use of sensor embedded gloves that can quantify the movement kinematics—movement range, joint velocity (angular/linear), quality of movement, etc., of the human hand. Glove based systems reduce the time and

effort needed for the assessment and enable easy assessment of functional tasks. Kinematic data obtained from glove based systems can be recorded for further analysis. Glove based systems are widely known as *Data Gloves* and are being used in applications such as rehabilitation medicine, entertainment, education, 3D modeling, and virtual reality (VR).<sup>1</sup> Taylor and Curran<sup>2</sup> provided a brief summary of glove based and non-glove based systems that are used in hand rehabilitation. The authors also emphasize the need for a user specific glove design to meet the user and therapist expectations and provide a portable, affordable design using LEAP (LEAP sensor from Leap Motion Inc. USA) motion controllers.

In the last few decades, researchers have developed different types of *Data Gloves* for monitoring the hand function. Boian *et al.* described the design of a virtual reality system using the CyberGlove and Rutgers Master II-ND haptic glove for the rehabilitation of chronic stroke patients.<sup>3</sup> Chuang *et al.* presented the design of a virtual reality based data glove equipped with fiber optic finger bend sensors for the objective analysis of the hand function.<sup>4</sup> *Humanglove* was developed for the functional assessment and monitoring of the hand function during the course of rehabilitation.<sup>5</sup> The design of a grasp-assistive glove was proposed and was used along with either a functional electrical muscle

<sup>a)</sup>Electronic mail: akhilmohan@cmcvellore.ac.in

<sup>b)</sup>Electronic mail: tharion@cmcvellore.ac.in

<sup>c)</sup>Electronic mail: rkkumar@iitm.ac.in

<sup>d)</sup>Electronic mail: surdev@cmcvellore.ac.in

stimulator or a robotic device (ADLER) for people with stroke.<sup>6</sup> The *Shadow Monitor*<sup>7</sup> and the *sensory glove*<sup>8</sup> use piezo-resistive sensors for the functional hand assessment, but the use of both these glove based systems is limited to the assessment of fingers. Park reported the design of a data glove and its performance analysis using a 3D graphic interface for the upper-extremity (fingers and wrist) rehabilitation.<sup>9</sup> Golomb *et al.* presented the results of home based virtual reality telerehabilitation for children and adolescents with cerebral palsy using a 5DT glove.<sup>10</sup> The accessibility and lower cost for in-home therapy may benefit the study population on a large scale and have to be addressed systematically. We have reported earlier the results of the design of a sensorized glove equipped with piezo-resistive sensors, optical linear encoders, and a 3-axis accelerometer for monitoring hand rehabilitation therapy for people with stroke.<sup>11</sup> Friedman *et al.*<sup>12,13</sup> presented the design of a wearable glove (“Music Glove”) for training isometric grip and functional hand movements. O’Flynn *et al.*<sup>14</sup> presented the design of a smart glove for monitoring the hand function, but it is only suitable for able bodied individuals. Shin *et al.*<sup>15</sup> described the use of the Rapael Smart Glove with VR for providing hand rehabilitation therapy. Although the results are promising, the expensive price of the glove along with accessories limits its use for a wider population. Placidi *et al.* proposed a virtual glove system using two orthogonal LEAP motion controllers for the rehabilitation of the stroke hand.<sup>16</sup>

A comparison of commercially available glove based systems is also presented here (see Table I).

The major drawbacks of the existing Data Gloves are

- Poor usability of the device—Donning and doffing of glove should be made easier for people with neurological impairments and musculoskeletal disorders.
- Poor portability to rural/home based settings—Home based devices will provide more access to hand

rehabilitation therapy and will lower the cost associated with the therapy.

In this paper, we present the design of an inertial motion sensor based, portable instrumented glove (i-Glove) for people with neurological impairments and musculoskeletal disorders. The i-Glove is designed to

1. Measure the distal hand function of people with neurological impairments
  - Measurement of clinically relevant features (range of motion, tremor, etc.).
2. Monitor the continuous movement of the hand in the physiological range.

The device can be employed in a variety of clinical settings where the objective is to (a) quantify and evaluate the effectiveness of a clinical intervention to improve the hand function or (b) to complement clinical intervention, for example, by a direct biofeedback or by using the i-Glove data to drive an interactive virtual reality game.

## II. METHODS

During physical rehabilitation therapy, gross hand movements are developed during the initial stages of motor recovery and are followed by fine movements. The therapist would like to optimize the hand rehabilitation therapy for training patients. The requirement of a portable hand rehabilitation device which can track the effect of hand rehabilitation forms the design requirements of the i-Glove and are listed based on its degree of importance in Table II.

In Table II, IP = Inter-Phalangeal joint, CMC = Carpo-Meta-Carpal joint, DIP = Distal Inter-Phalangeal joint, PIP = Proximal Inter-Phalangeal joint, MCP = Meta-Carpo-Phalangeal joint, RC = Radio-Carpal joint, and RU = Radio

TABLE I. Comparison of glove based systems with *HandREPS*.

Device	Sensor	Precision	Interface	Features	Cost
Raphael Smart Glove <sup>17</sup>	Bend sensors and IMU	NA	Wireless	Capture motion and posture, train functional movements, very expensive	\$15 000
Cyber Glove II <sup>18</sup>	Piezo-resistive	<1 deg	USB, wireless	Calibration required, very expensive	\$12 295
5DT glove 5 ultra <sup>19</sup>	Fiber optic	10 bit	Serial, USB	Automatic calibration, wireless version available, cross-platform SDK (Windows, Linux and Mac)	\$995
DG5 VHand 3.0 <sup>20</sup>	Piezo-resistive	4 bit	USB and Wi-Fi	Can fit any hand size, cannot measure small hand movements, time consuming setup	\$800
VMG8/VMG30 <sup>21,22</sup>	Bend sensors	12 bit	USB, Bluetooth	Calibration required, provide complete SDK for custom design, provide full network support to run the application using the data from an another machine	\$500
AcceleGlove <sup>23</sup>	Dual axis accelerometer	6.5 deg	USB	No calibration, wireless version available, arm tracking with optional component	\$499
Music Glove <sup>12,13</sup>	Electrical contacts	10N	USB	Lightweight, trains functional hand movements	\$399
LEAP <sup>24</sup>	Dual IR cameras	32 bit	USB	No calibration required, low cost, limited to healthy subjects	\$80
HandREPS	MARG sensors, absolute pressure sensor	<5 deg	Bluetooth	Calibration required, portable, can fit any hand size, anatomical joint angle measurement in a moving co-ordinate frame	<\$250

TABLE II. Joint articulations of hand and its degree of importance.

Joint	Segment	Movement	Priority
IP	Thumb	F/H	High
CMC	Thumb	F/E	High
	Thumb	Ad/Ab	Intermediate
	Thumb	Opposition	High
DIP	Index	F/E	Low
	Middle	F/E	Low
	Ring	F/E	Low
PIP	Index	F/E	High
	Middle	F/E	High
	Ring	F/E	Low
	Little	F/E	Low
MCP	Thumb	F/E	High
		Ad/Ab	Intermediate
	Index	F/E	High
		Ad/Ab	Intermediate
	Middle	F/E	High
		Ad/Ab	Intermediate
	Ring	F/E	Low
		Ad/Ab	Low
	Little	F/E	Low
		Ad/Ab	Low
RC	Wrist	F/E	High
	Wrist	Ad/Ab	Intermediate
RU	Wrist	P/S	High

Ulnar joint; F/H = flexion/hyperextension, F/E = flexion/extension, Ad/Ab = adduction/abduction, and P/S = pronation/supination.

### A. Instrument design

Our i-Glove uses MARG (Magnetic, Angular Rate and Gravity) sensors placed across the joints of interest in the fingers and the wrist. The block schematic representation of the i-Glove is shown in Fig. 1. For biomechanical assessment, the convention is to represent the rotation of the distal segment with respect to the proximal segment. For example, flexion of the wrist is the angle of the hand (distal segment) to the forearm (proximal segment), as shown in Fig. 2, and rotation of the forearm is the rotational angle of the forearm (distal segment) with respect to the upper arm (proximal segment). The orientation data obtained from the MARG sensors are thus expressed in body coordinates or in an anatomical co-ordinate system. In the i-Glove, the relative Euler angles are then calculated from

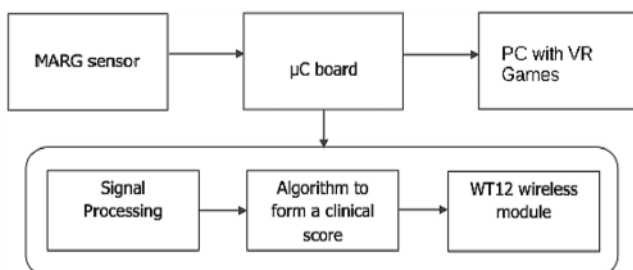


FIG. 1. Block level representation of the i-Glove.

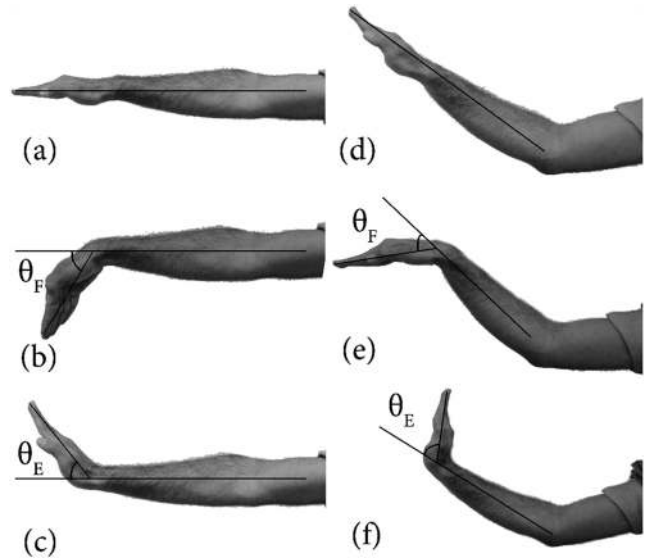


FIG. 2. Body or anatomical co-ordinate system used to understand wrist flexion/extension movement where  $\theta_F$  represents wrist flexion and  $\theta_E$  represents wrist extension.

the body coordinates (anatomical co-ordinates) and sent every 40 ms to a computer, wirelessly using a Bluetooth device.

The i-Glove is fitted with TDK-Invensense MPU9250 (MARG sensor) to measure the kinematics of the hand. The data from the MARG sensors are read by a Microchip dsPIC33FJ128GP804 microcontroller, which calculates joint angles, as listed in Table II. The joint angles are then sent to a Personal Computer (PC) using Bluegiga WT12 Bluetooth® Class 2 module. The complete system runs on a Nokia® BL-5C Li-ion battery, and the average current drawn is about 150 mA (Fig. 3) which translates to about 6.8 h of use on a fully charged battery with a capacity of more than 1020 mAh—daily recharging is recommended.

Apart from measuring the segment joint angle described in Table III, the i-Glove also measures the angular velocity and linear acceleration of the segment on which MARG sensors are attached. The quality of movement (presence or absence of tremor and control of movement) and the speed of movement can be derived using this data and could be used to tailor the rehabilitation therapy. Focused, patient specific rehabilitation therapy can benefit the user to maximize functional independence and improve the quality of life of individual.



FIG. 3. i-Glove designed for hand rehabilitation/assessment.

TABLE III. i-Glove capability to measure joint articulations of the hand with a higher degree of importance described in Table II.

Joint	Segment	Movement	Capability
IP	Thumb	F/H	Yes
CMC	Thumb	F/E	No
	Thumb	Opposition	No
PIP	Index	F/E	Yes
	Middle	F/E	Yes
MCP	Thumb	F/E	Yes
	Index	F/E	Yes
	Middle	F/E	Yes
RC	Wrist	F/E	Yes
RU	Wrist	P/S	No

## B. User oriented glove design for segment joint angle measurement

Many of the existing glove based devices are designed for people with good articulation of the hand which means the fingers can be flexed to slip into the glove. People with musculoskeletal disorders or impaired hand may have rigidity of the fingers, and the fingers may be bent in a claw-like manner due to the impairment. They find it difficult to don a full glove and need a modified glove which can be fitted easily producing minimal discomfort.

Our design of a wearable “glove” is in the form of flexible finger rings which can be attached to the digits using Velcro straps and produce little or no discomfort to the user. If the attachment of rings with Velcro is difficult due to anatomical constraints (e.g., distal segment of the thumb), clinical grade adhesive paper tape (e.g., *micropore*) is used in our experiments. The center of the sensor is about 10 mm from the center of the finger joints and about 40 mm in the case of wrist joint. The attachment of MARG sensors on the finger and wrist to measure hand movements is shown in Fig. 4.

## C. MARG sensor calibration

The MARG sensors need to be calibrated to determine the scale factor and offset (bias) of the individual sensor modules—linear accelerometer, gyroscope, and magnetic

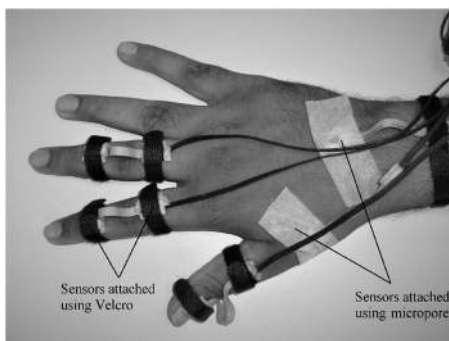


FIG. 4. Placement of MARG sensors on the hand to measure the finger joint angle.

compass. For a linear sensor model, we use Eq. (1).

$$\begin{bmatrix} M_x \\ M_y \\ M_z \end{bmatrix} = \begin{bmatrix} \frac{1}{S_x} & 0 & 0 \\ 0 & \frac{1}{S_y} & 0 \\ 0 & 0 & \frac{1}{S_z} \end{bmatrix} \begin{bmatrix} R_x \\ R_y \\ R_z \end{bmatrix} - \begin{bmatrix} \frac{B_x}{S_x} \\ \frac{B_y}{S_y} \\ \frac{B_z}{S_z} \end{bmatrix}. \quad (1)$$

Here  $M_x$ ,  $M_y$ , and  $M_z$  are the calibrated sensor module (accelerometer or gyroscope or magnetic compass) data, and  $R_x$ ,  $R_y$ , and  $R_z$  are the corresponding uncalibrated data from the sensor module under test in  $x$ ,  $y$ , and  $z$  directions.  $B_x$ ,  $B_y$ , and  $B_z$  are the offset (bias), and  $S_x$ ,  $S_y$ , and  $S_z$  are the sensitivity (scaling factor) of the sensor module under test in  $x$ ,  $y$ , and  $z$  directions.

### 1. 3-Axis accelerometer

The accelerometer calibration was performed on a leveling platform using a 6-point tumble test. The 3-axis accelerometer data are recorded at 40 Hz from each axis and are averaged to obtain a single value corresponding to the experiment. The experiment was repeated thrice on each axis, and the average value was used to determine the bias and sensitivity of the accelerometer.

### 2. 3-Axis gyroscope

The gyroscope is calibrated using a rotary rate table (on a CNC machine). The rotary table is rotated at three known angular speeds (low—10°/s, medium—20°/s, and high—33°/s), and the 3-axis gyroscope data are recorded at 40 Hz. The data collected from the three angular speeds are averaged to obtain a single value which was used to determine the bias and sensitivity of the accelerometer.

### 3. 3-Axis magnetic compass

To minimize the effect of magnetic substances in the vicinity during measurement using a magnetic compass, the 3-axis compass is subjected to calibration. To obtain the hard iron bias and soft iron bias (scaling factor), the sensor is moved in space forming a 3D-hyper sphere. The 3-axis magnetic sensor was configured to collect data at 40 Hz.

## D. Orientation estimation using MARG sensor

Even though we have calibrated all three sensors (accelerometer, gyroscope, and magnetic compass), any one sensor itself cannot be reliably used for the estimation of the segment joint angle of the hand.

- A 3-axis accelerometer can be used to estimate the rotation about the  $x$ -axis and  $y$ -axis under static conditions
- A 3-axis gyroscope can be used to calculate the rotation about the  $x$ -axis,  $y$ -axis, and  $z$ -axis under dynamic conditions
- In a homogeneous magnetic field, a 3-axis magnetic compass can be used to measure rotational vectors orthogonal to earth’s magnetic field

The use of any sensor alone for a prolonged duration results in large orientation errors due to inherent sensor noise (drift) arising due to different factors (mechanical, thermal,

and electrical) and errors due to finite numerical word length. So, in general, we combine the information from two or three sensors to minimize the error; this is known as “*Sensor Fusion*” to predict a better measure of the joint angle. Several sensor fusion algorithms have been developed for orientation estimation in the presence of noise, and well known among them are Kalman filters<sup>25,26</sup> and complementary filters.<sup>27</sup> A method proposed by Madgwick *et al.* referred to as the “Madgwick Filter” has been implemented in the i-Glove. The data from the calibrated sensor modules (accelerometer, gyroscope, and magnetic compass) are combined to obtain the quaternion representing the orientation of the sensor with respect to North-East-Down (NED) sampled at time  $t$  (the sensor orientation in NED co-ordinates is indicated by prefixed superscript  $S$  representing the sensor frame and prefixed subscript  $E$  representing the Earth frame, and therefore, the quaternion estimate at time  $t$  is written as  ${}^S_E q_{est,t}$ ),<sup>28</sup>

$${}^S_E q_{est,t} = {}^S_E \hat{q}_{est,t-1} + {}^S_E \dot{q}_{est,t} \times \Delta t, \quad (2)$$

$${}^S_E \dot{q}_{est,t} = {}^S_E \dot{q}_{\omega,t} - \beta \frac{\nabla f}{\|\nabla f\|}. \quad (3)$$

Here  ${}^S_E \hat{q}_{est,t-1}$  is the previous estimate of orientation,  ${}^S_E \dot{q}_{est,t}$  is the rate of change of orientation, and  $\Delta t$  is the sampling period. The results from the 3-axis gyroscope calibration are used to determine the gyroscope measurement error; the correction coefficient  $\beta$  minimizes the error in the rate of change of orientation obtained using the gyroscope change ( ${}^S_E \dot{q}_{\omega,t}$ ).  $f$  is the objective function based on accelerometer and magnetometer measurements, and the symbol  $\nabla$  indicates the gradient; the objective function is calculated using the gradient descent.

### E. Euler angle estimation

The quaternion representing the sensor orientation with respect to the global co-ordinate system (GCS) as in Fig. 5 obtained using the Madgwick filter is used to determine the absolute Euler angles (YZX order). Singularities in the calculation occur when we try to convert the quaternion data to the Euler angle form. To resolve this problem, we hard-coded the value of the rotation about the z-angle ( $\psi$ ) around the singularity region at  $90^\circ$  (i.e., to avoid division by zero).

For biomechanical analysis, the convention is to use the relative joint angle where the rotation of a distal segment is described with respect to the proximal segment. To obtain the relative joint angle, first the quaternions representing the sensor orientation with respect to the GCS are expressed in

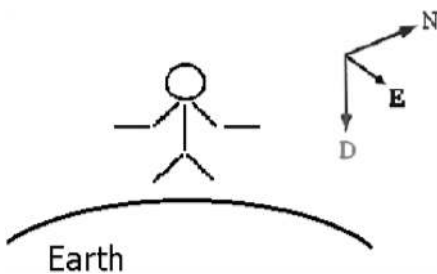


FIG. 5. MARG sensor axis alignment in the NED global co-ordinate frame.

the anatomical coordinate system or body coordinate system (BCS). The sensor to segment calibration is performed for the same and is summarized in Sec. II E 1. The quaternions representing the sensor orientation with respect to the BCS are used to determine relative joint angles and are described in Sec. II E 2.

### 1. Sensor to segment (fingers/wrist) calibration

Rotations are presented using Euler angles. For a clearer interpretation of Euler angles, the proximal and distal segments describing the movements are initially aligned to each other. The rotation of the distal segment is described with respect to the proximal segment to obtain the clinically pertinent parameters (flexion/extension/hyperextension, adduction/abduction, and pronation/supination).<sup>29</sup> For the same, the quaternion representing the orientation of the MARG sensor with respect to the GCS needs to be expressed in terms of the BCS. So a static pose (position where the orientation of the proximal and distal segments is aligned) is assumed initially where the hand is kept on a flat neutral position aligning the z-axis with the direction of gravity,

$${}^B_E q_{est,t} = {}^S_E q_{est,t} \otimes {}^S_B q'_{est,t}. \quad (4)$$

Here  ${}^B_E q_{est,t}$  is the quaternion representing the orientation of the body with respect to the NED frame,  ${}^S_E q_{est,t}$  is the quaternion representing the orientation of the sensor with respect to the NED frame, and  ${}^S_B q'_{est,t}$  is the quaternion conjugate representing the orientation of the sensor with respect to the anatomical or body co-ordinate system. The symbol  $\otimes$  denotes quaternion multiplication.

### 2. Representation of Euler angle for biomechanical analysis

The quaternion representing the sensor orientation with respect to the BCS obtained from the sensor to segment calibration is used to determine relative joint angles. In Fig. 6, the quaternion representing the orientation of the proximal segment ( $q_P$ ) is MARG 2 and the quaternion representing the orientation of the distal segment ( $q_D$ ) is MARG 1. Here,

- The negative x-axis directed distally (tip of the middle finger)
- The positive z-axis directed dorsally
- The negative y-axis directed radially (orthogonal to X-Z)

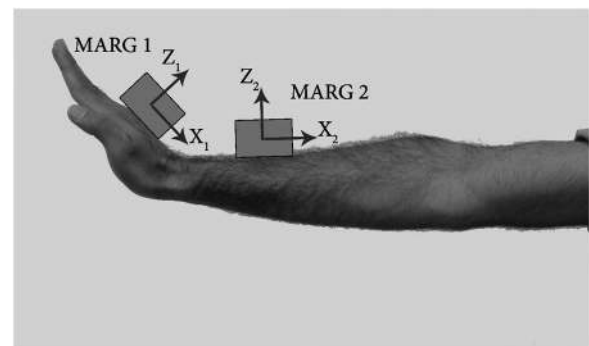


FIG. 6. MARG sensor axis alignment in the anatomical or body co-ordinate system.

The relative quaternion representing orientation of the distal segment with respect to the proximal segment is obtained using Eq. (5),

$${}^D_P q_{est,t} = q_{P_{est,t}}^* \otimes q_{D_{est,t}}. \quad (5)$$

Here  $q_P^*$  is the conjugate of  $q_P$ . The quaternion  ${}^D_P q_{est,t}$  is then used to determine joint angles (YZX order). In Fig. 6, the rotation of Z1 with respect to Z2 forms wrist abduction and adduction and the rotation of Y1 with respect to Y2 forms wrist flexion/extension.

## F. Calibration of Euler angle

Complex calibration methods for the evaluation of MARG sensors have been proposed by various researchers,<sup>30–33</sup> and the results from these calibrations are not easily interpretable for use in rehabilitation therapy. We present a simple, reliable calibration (static and dynamic) method using potentiometers to obtain the reference values to evaluate the performance of MARG sensor(s) measuring Euler angle(s). The block level representation of the experimental setup to calibrate the MARG sensor(s) is shown in Fig. 7. We employ MARG sensor(s) and rotary potentiometers for the measurement of the rotation angle continuously. The rotation angles are sent to the PC wirelessly using a Bluetooth device every 20 ms (i.e., 50 Hz sampling) during static calibration and 25 ms (i.e., 40 Hz sampling) during dynamic calibration. A triple pendulum arrangement comprising 3 links, each with one degree of freedom (DoF) rotating about orthogonal axes, as shown in Fig. 8, is used for the calibration of the MARG sensor.

To determine the static accuracy of the MARG sensor, we performed a calibration routine (static and dynamic) where the rotation of the MARG sensor about x-, y-, and z-axes is recorded on a computer. During the calibration of the MARG sensor, the rotation about the x-axis (roll) and y-axis (pitch) was measured between  $-180^\circ$  and  $+180^\circ$  and the rotation about the z-axis (yaw) was measured between  $-90^\circ$  and  $+90^\circ$ . The dynamic calibration at frequencies (0.2 Hz, 0.4 Hz, 0.6 Hz, and 0.75 Hz) was performed using the experimental setup described in Fig. 8. Here, the distal segment was manually moved in time to a metronome and the process was performed on x-, y-, and z-axes. Note that this triple pendulum gives a human limb like co-ordinate system (anatomical co-ordinate system), and each limb's origin moves when the preceding limb moves. Segment 1 represents the hand, segment 2 represents the forearm, and segment 3 represents the upper arm

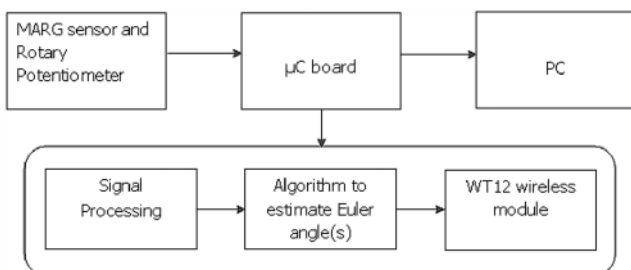


FIG. 7. Block level representation of i-Glove calibration.

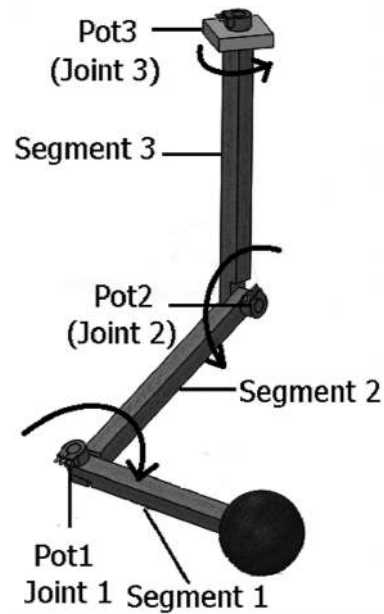


FIG. 8. Experimental setup to calibrate the MARG sensor for measuring the joint angle.

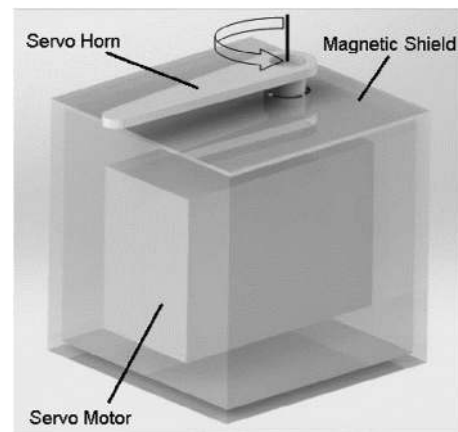


FIG. 9. Dynamic calibration experimental setup.

in the triple pendulum arrangement measuring wrist flexion/extension (Pot 1), elbow flexion/extension (Pot 2), and shoulder internal rotation/external rotation (Pot 3).

Dynamic calibration was also performed using a servo motor (Fig. 9) at frequencies of 0.25 Hz, 0.5 Hz, and 1.0 Hz. The servo motor gives better sinusoidal waveforms for a single degree of freedom, while the triple pendulum gives multiple degrees of freedom in an anatomical co-ordinate system. The servo motor was kept inside a magnetic shield so that it did not present a time or space varying magnetic field to the magnetometer in the MARG sensor. The MARG sensor was placed on the servo horn and rotated only about the z-axis from  $-60^\circ$  to  $+60^\circ$ .

## III. RESULTS AND DISCUSSION

### A. Sensor module calibration

The sensor data are scaled appropriately, and the bias is subtracted from the raw measurement. The data from the

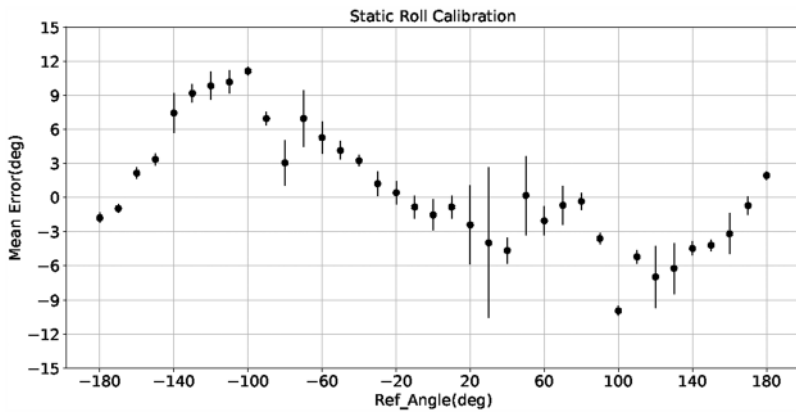


FIG. 10. Static calibration of the MARG sensor (roll); mean error and standard deviation are as outcome measures.

sensor modules are combined using the filter fusion algorithm to produce quaternion representing the orientation of the MARG sensor with respect to the anatomical or body coordinate system. The orientation from the sensor data is used to determine Euler angles in real time.

**B. Results of Euler angle calibration**

The static calibration was performed to obtain the measurement error of the MARG sensor. The MARG sensor was subject to rotate between  $-180^\circ$  and  $+180^\circ$  for roll and pitch and  $-90^\circ$  to  $+90^\circ$  for yaw in steps of  $10^\circ$ . At each orientation, the data were recorded for about 20 s (data points  $\approx 1000$ ) and were used to calculate the mean error and standard deviation. The changes in the mean error and standard deviation during

the static calibration of the MARG sensor over two trials (forward where the pendulum was moved from the negative extreme limit to positive extreme limit and backward where the pendulum was moved from the positive extreme limit to negative extreme limit) are shown in Figs. 10–12. The mean absolute error (mae) and root mean squared error (rmse) are used as the performance measures and are shown in Table IV.

The dynamic calibration at frequencies 0.2 Hz, 0.4 Hz, 0.6 Hz, and 0.75 Hz was performed using the same experimental setup described in Fig. 8. Here, the distal segment was moved manually in time to a metronome and the process was performed for the rotation about x, y, and z axes. As noted in Sec II, the rotation axes are relative to the preceding limb segment. The summary of the results of the dynamic calibration is described in Table V.

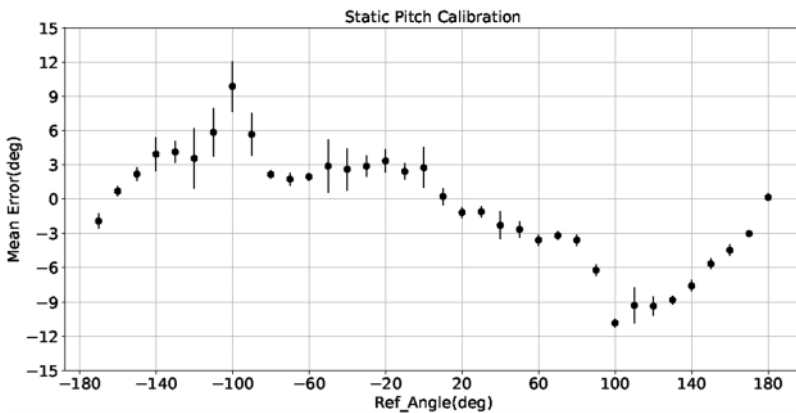


FIG. 11. Static calibration of the MARG sensor (pitch); mean error and standard deviation are as outcome measures.

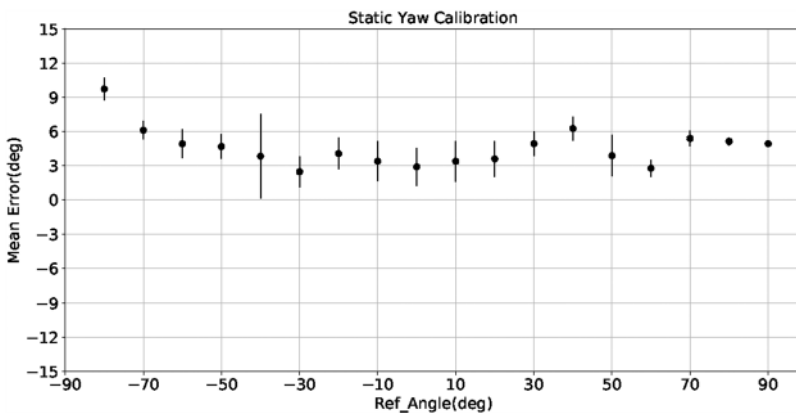


FIG. 12. Static calibration of the MARG sensor (yaw); mean error and standard deviation are as outcome measures.

TABLE IV. Results of Euler angle calibration—static; mae and rmse correspond to the mean absolute error and root mean squared error, respectively.

Feature	x-axis (deg)	y-axis (deg)	z-axis (deg)
mae [rmse]	4.1[5.1]	4.0[4.9]	4.6[6.5]

TABLE V. Results of Euler angle calibration—dynamic; mae and rmse correspond to the mean absolute error and root mean squared error, respectively.

Feature	Freq (Hz)	x-axis (deg)	y-axis (deg)	z-axis (deg)
mae [rmse]	0.2	7.7[8.3]	3.8[4.7]	4.5[5.0]
	0.4	9.5[11.3]	6.6[7.5]	7.6[8.6]
	0.6	9.9[12.2]	7.4[8.7]	10.2[11.6]
	0.75	10.1[12.1]	14.9[17.8]	12.8[14.5]

The second method of dynamic calibration was performed on the z-axis using a servo motor assembly (Fig. 9) at frequencies 0.25 Hz, 0.5 Hz, and 1.0 Hz. The MARG sensor was placed on the servo horn and rotated about the z-axis from  $-60^\circ$  to  $+60^\circ$ . The dynamic calibration using the triple pendulum arrangement and servo motor shows similar results and is shown in Fig. 13.

The summary of the dynamic calibration of the estimated yaw angle measured using the MARG sensor in comparison with the rotary potentiometer is given in Table VI where the gain was obtained by taking the ratio of angle (peak value) obtained from the MARG sensor ( $\theta_{MARG}$ ) with the angle measured using the rotary potentiometer ( $\theta_{Pot}$ ). A gain close to one indicates that the output angle measured using the MARG sensor ( $\theta_{MARG}$ ) was able to track the input angle ( $\theta_{Pot}$ ) during calibration.

A third method of dynamic calibration was performed by the fast release of the limb with the sensor (in the direction of the pitch angle), and the response of the MARG sensor was measured. The results are shown in Fig. 14. We measured the overshoot and convergence time from this, and they were  $17^\circ$  and 0.4 s, respectively.

The dynamic calibration of the MARG sensor with sinusoidal inputs and step inputs is used to describe the system characteristics which are summarized below.

- **Overshoot**—At 0.2 Hz, the estimated yaw angle closely follows the reference trajectory obtained from the

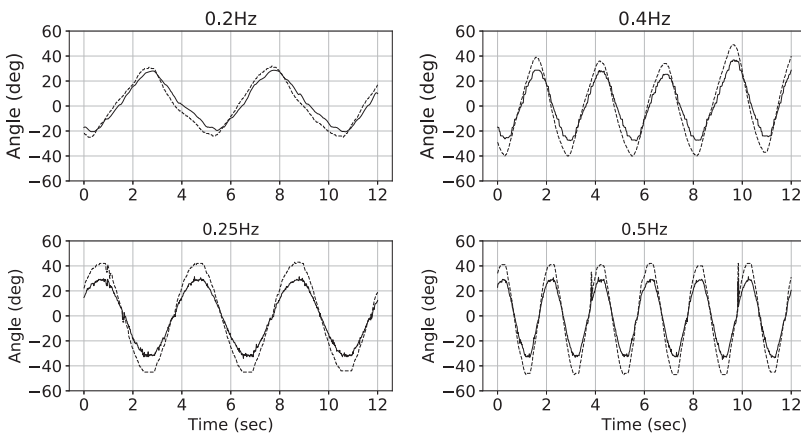


FIG. 13. Dynamic calibration of the MARG sensor (yaw) using the triple pendulum arrangement (0.2 Hz and 0.4 Hz) and servo motor assembly (0.25 Hz and 0.5 Hz); dotted line is the angle measured using the MARG sensor, and the bold line is the angle measured using a rotary potentiometer.

TABLE VI. Comparison of the efficiency of the angle (peak value) measured using the MARG sensor with a rotary potentiometer during dynamic calibration;  $\theta_{Pot}$  and  $\theta_{MARG}$  are measured when yaw attains the maximum value.

Frequency (Hz)	$\theta_{Pot}$ (deg)	$\theta_{MARG}$ (deg)	Gain
0.2	30	32	1.07
0.25	30	39	1.30
0.4	30	37	1.23
0.5	30	40	1.33
0.6	30	42	1.40
0.75	30	42	1.40
1.0	30	40	1.33

rotary potentiometer (Fig. 15). The rotation angle (yaw) obtained during the dynamic calibration shows that the filter fusion algorithm overestimates the yaw angle (peak value) by a factor of  $\sim 1.35$  at frequencies higher than 0.2 Hz. The dynamic response depends on both the sensor response to the input and the algorithm/computation time that the processor takes to converge while estimating the Euler angle.

- **Convergence time**—The step response experiment measured an overshoot of  $17^\circ$  and a convergence time of 0.4 s (Fig. 14). The convergence time of 0.4 s indicates the dynamic range in which the sensor could be reliably used (0-2.5 Hz) in the clinical settings to quantify physiological parameters (tremor and smoothness).
- **Phase response**—Filter fusion algorithms in general try to minimize the difference between the instantaneous input value and output value. However, due to errors in estimation, the instantaneous error can be positive or negative. For example, the rotation angle (yaw) obtained during the dynamic calibration has phase shifts of  $3.6^\circ$  at 0.4 Hz movement sampled at 40 Hz and  $2.8^\circ$  at 0.5 Hz movement sampled at 64 Hz (Fig. 16). This can sometimes produce an apparent phase lag/lead or time delay/advance. However, this cannot be interpreted in the same way as for a minimum-phase linear system, or even a linear system with a fixed delay (non-minimum phase).

It is easy to think of measurement systems in terms of linear system terminology. Movement speed can be described

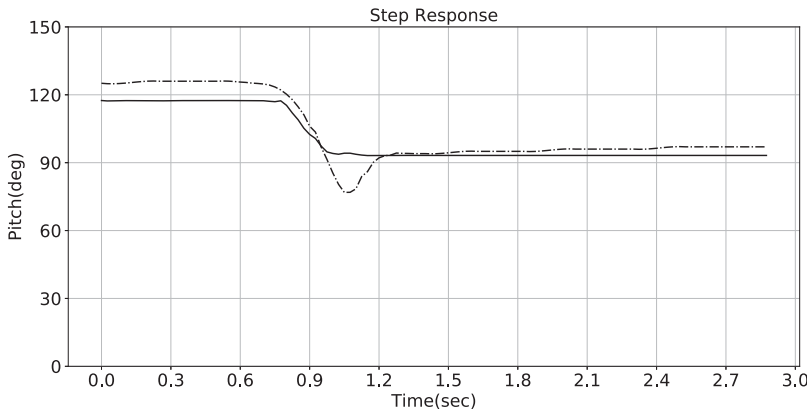


FIG. 14. Step response of the MARG sensor; dotted line is the angle measured using the MARG sensor, and the bold line is the angle measured using a rotary potentiometer.

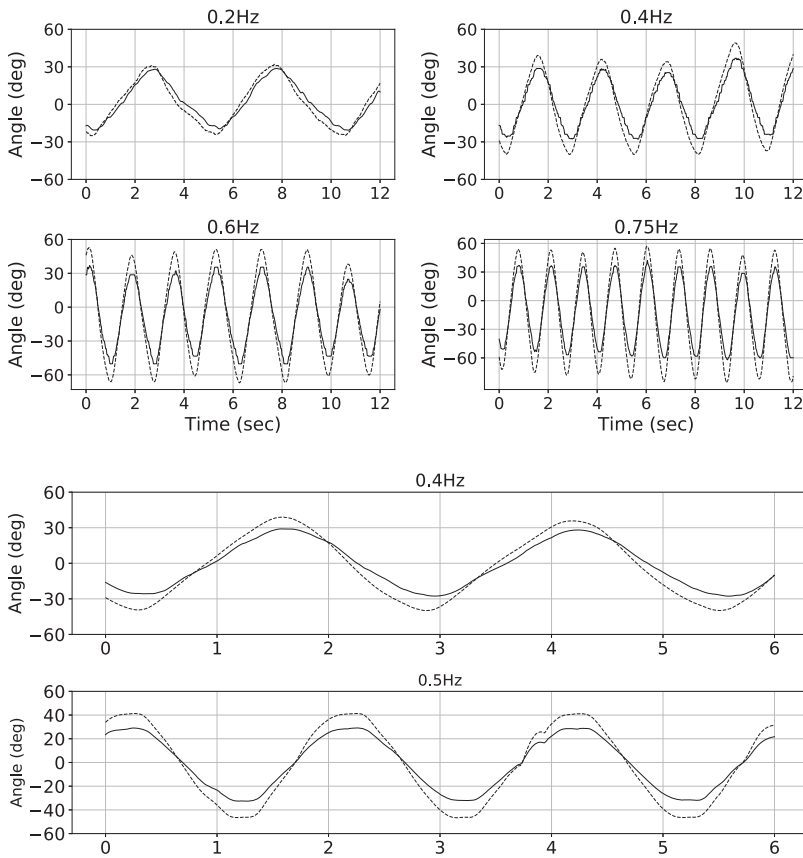


FIG. 15. Dynamic calibration of the MARG sensor performed using the pendulum assembly (yaw); dotted line is the angle measured using the MARG sensor, and the bold line is the angle measured using a rotary potentiometer.

in terms of trajectories and the frequency composition of the trajectories. So it is useful to express the system parameters in terms of amplitude gain, phase lag, and convergence time along with the mean absolute error/root mean squared error when MARG sensors are used for orientation estimation.

**C. Results of relative joint angle calibration**

A static calibration was performed to obtain the system characteristics (measurement error) during the estimation of the relative joint angle or anatomical angle. We rotate the distal segment with respect to the proximal segment between  $-180^\circ$  and  $+180^\circ$  for wrist flexion/extension (relative roll) and elbow flexion/extension (relative pitch) and  $-90^\circ$  to  $+90^\circ$  for shoulder internal rotation/external rotation (relative yaw), and the results were recorded on a PC sampled at

40 Hz. The results from the static calibration are shown in Table VII.

The dynamic calibration was performed at frequencies 0.25 Hz, 0.5 Hz, 0.8 Hz, and 1.1 Hz movement using the experimental setup described in Fig. 8. For this calibration method, the speed of the distal segment is set to be in sync with a metronome and the process was performed on the relative x, y, and z axis. The data were sampled at 40 Hz, and the

TABLE VII. Results of the relative joint angle (RR—Relative Roll, RP—Relative Pitch, and RY—Relative Yaw) calibration—static; mae and rmse correspond to the mean absolute error and root mean squared error, respectively.

Feature	RR (deg)	RP (deg)	RY (deg)
mae [rmse]	6.3[6.7]	5.0[6.8]	4.5[6.1]

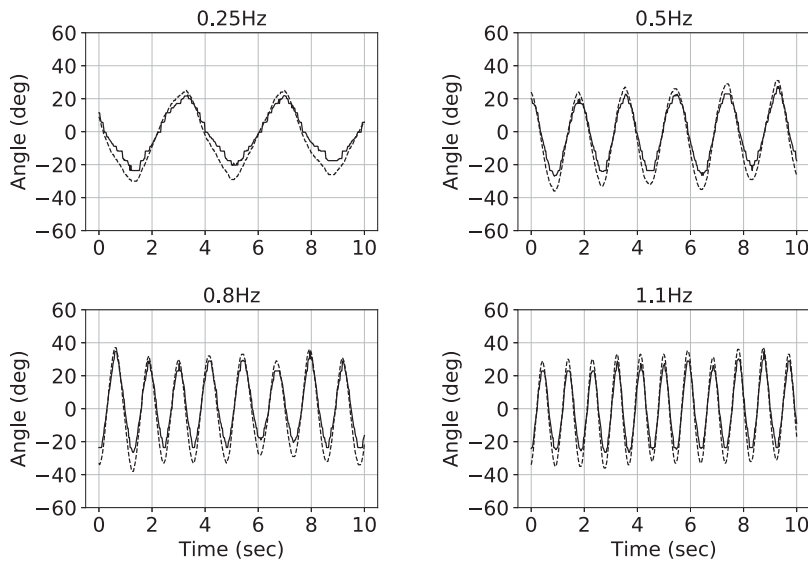


FIG. 17. Dynamic calibration of the MARG sensor pair performed using the pendulum assembly (relative yaw); dotted line is the angle measured using the MARG sensor pair, and the bold line is the angle measured using a rotary potentiometer.

results of the dynamic calibration are shown in Fig. 17. The summary of the results of the dynamic calibration is described in Table VIII.

At 0.25 Hz, the estimated relative joint angle closely follows the reference trajectory obtained from the rotary potentiometer. The relative yaw (adduction/abduction) obtained during the dynamic calibration shows that the filter fusion algorithm overestimates the joint angle (peak value) by a factor of  $\sim 1.25$  at frequencies higher than 0.25 Hz. The estimated joint angle is satisfactory over the range of clinical interest (0-3 Hz of movement) and can be used as a device for monitoring the hand function.

The inherent resolution of the accelerometer is 0.0001 g or 0.001 m/s<sup>2</sup>; the inherent resolution of the gyroscope is 0.015°/s; the inherent resolution of the magnetic compass is 0.0732  $\mu$ T. After the computation through the algorithm, anatomical joint angles were calculated and are reported in Table VII (results of static calibration) and Table VIII (results of dynamic calibration). The accelerometer and gyroscope data are sampled at 500 samples/s, and magnetic compass data are sampled at 100 samples/s. The accelerometer and gyroscope data undergo preprocessing (block averaging and down sampling by a factor of 20) before they are fed to the filter fusion algorithm. The output from the filter fusion algorithm has a sampling rate of 25 samples/s. The errors described from the calibration experiments are a combination of sensor errors, algorithm errors, and arithmetic/numerical errors.

TABLE VIII. Results of the relative joint angle (RR—Relative Roll, RP—Relative Pitch, and RY—Relative Yaw)—dynamic; mae and rmse correspond to the mean absolute error and root mean squared error, respectively.

Feature	Freq (Hz)	RR (deg)	RP (deg)	RY (deg)
mae [rmse]	0.25	9.5[9.8]	3.9[4.7]	4.2[5.0]
	0.5	11.6[12.0]	4.6[5.6]	4.9[5.7]
	0.8	10.0[10.7]	5.3[6.3]	5.4[6.4]
	1.1	10.2[11.2]	6.3[7.5]	5.4[6.2]

#### IV. CONCLUSION

We have presented the design of an instrumented glove equipped with Magnetic, Angular Rate and Gravity sensors for the objective evaluation of the hand function for people with neurological impairment. The i-Glove presented in this paper can assess both the range of movement of the user's hand and continuous anatomical joint angles. It can be used to monitor the functional recovery of motor control in the hand during the course of hand rehabilitation. The i-Glove presented in this paper has several advantages over the existing devices. Two important contributions of this paper are

1. Measurement of anatomical joint angles in a moving coordinate frame
  - While the use of flex sensors and potentiometers makes joint angle measurement straightforward, they are inconvenient compared to MARG sensors placed on the paretic hand. Flex sensors and potentiometers make assumptions about the joint center of rotation that are not required when using MARG sensors. Therefore a method using MARG sensors gives an angle measurement with the accuracy suitable for rehabilitation therapy which is an important development.
2. Novel methods for dynamic calibration in such situations
  - There is no report of a simple and reliable dynamic calibration experiment in the literature. Researchers performed different methods ranging from using a simple metronome to complex servo motor for calibrating MARG sensors as described in Refs. 34 and 35. A simple, reliable calibration (static and dynamic) method using a potentiometer provides a better representation of the true angle. Such calibration has been used to evaluate the performance of MARG sensor(s) measuring Euler angle(s) in real time.

The mean absolute error during the static calibration for all three attitude changes, namely, roll, pitch, and yaw, is less than  $4.6^\circ$ . During dynamic movement, a rapid change in the angle gives a convergence time of 0.4 s, and for pure frequencies less than 0.25 Hz, there is less than 7% error in tracking of the angle. We have also calibrated the estimation of the anatomical joint angle, that is, the angular change clinically referred to as flexion/extension movement of the wrist and elbow and shoulder internal rotation/external rotation. These angular measures are changes in a distal segment of a limb with reference to its adjacent proximal segment. Therefore, such angles use a relative co-ordinate system. When using such a relative co-ordinate system, there is the danger of ambiguous angle estimation when the proximal segment has changed the co-ordinate system by more than  $90^\circ$ . We have also presented the results for such anatomical angle measurements as the static and dynamic calibration of the instrumented glove (a sensor pair measuring one joint angle). The mean absolute error during static calibration was  $6.3^\circ$  for wrist flexion/extension,  $5.0^\circ$  for elbow flexion/extension, and  $4.5^\circ$  for shoulder internal rotation/external rotation.

The preliminary results from the instrumented glove are promising and could be used as an alternative to the traditional therapist assisted hand rehabilitation along with interactive virtual reality computer games. In conventional physical therapy for rehabilitation, the assessment and the therapy are usually separate as it is difficult to use protractors, mechanical goniometers, and dynamometers during the therapy activity. The i-Glove estimates the anatomical angles continuously and unobtrusively and can be readily used during therapy. The i-Glove not only can be used during conventional physical therapy, but also can be incorporated in virtual reality based computer games which can be more engaging and interesting for the patient undergoing therapy. By reducing the routine work for physiotherapists, the i-Glove also enables them to design more interesting, intensive, and fruitful therapy regimes. In such a scenario where less attention is demanded from the clinical expert (physiotherapist), the cost of therapy will reduce and the quality and quantity of therapy can also increase.

The current version of the i-Glove is limited to the measurement of flexion and extension of the thumb, index finger, middle finger, and wrist. Measurement of flexion and extension of the remaining two fingers (ring finger and little finger), abduction/adduction movements of MCP joints, and wrist and radio ulnar movements can be readily performed if necessary. The additional measurement of these movements would also help us to monitor a wide range of motor activities and design patient specific rehabilitation treatments providing objective data of hand recovery.

The i-Glove described in this paper is currently being used to develop such therapy regimes with clinical experts, and preliminary versions are being tested by stroke patients undergoing hand rehabilitation therapy.

## ACKNOWLEDGMENTS

We wish to acknowledge the support of the students (Mr. Sandeep G, Mr. Sahil Gera, Mr. Aravind N, and Mr. Naveen G)

and staff (Mr. Parameswaran) from the Department of Bioengineering and Department of Physical Medicine and Rehabilitation, Christian Medical College, Vellore, and the Department of Biotechnology and Department of Engineering Design, Indian Institute of Technology Madras, for their support. A very special thanks to Kris Winer, Noel Hughes, S. Madgwick, and D. Roetenberg for their constant support and personal help.

- <sup>1</sup>L. Dipietro, A. M. Sabatini, and P. Dario, "A survey of glove-based systems and their applications," *IEEE Trans. Syst., Man Cybern., Part C* **38**(4), 461–478 (2008).
- <sup>2</sup>J. Taylor and K. Curran, "Glove-based technology in hand rehabilitation," in *Gamification: Concepts, Methodologies, Tools, and Applications*, edited by Information Resources Management Association (IGI Global, 2015), pp. 983–1002.
- <sup>3</sup>R. Boian, A. Sharma, C. Han, A. Merians, G. Burdea, S. Adamovich, M. Recce, M. Tremaine, and H. Poizner, "Virtual reality-based post-stroke hand rehabilitation," *Stud. Health Technol. Inf.* **85**, 64–70 (2002).
- <sup>4</sup>T. Y. Chuang, W. S. Huang, S. C. Chiang, Y. A. Tsai, J. L. Doong, and H. Cheng, "A virtual reality-based system for hand function analysis," *Comput. Methods Programs Biomed.* **69**(3), 189–196 (2002).
- <sup>5</sup>L. Dipietro, A. M. Sabatini, and P. Dario, "Evaluation of an instrumented glove for hand-movement acquisition," *J. Rehabil. Res. Dev.* **40**(2), 181–190 (2003).
- <sup>6</sup>D. E. Nathan, M. J. Johnson, and J. McGuire, "Design and validation of low-cost assistive glove for hand assessment and therapy during activity of daily living-focused robotic stroke therapy," *J. Rehabil. Res. Dev.* **46**(5), 587–602 (2009).
- <sup>7</sup>L. K. Simone, N. Sundararajan, X. Luo, Y. Jia, and D. G. Kamper, "A low cost instrumented glove for extended monitoring and functional hand assessment," *J. Neurosci. Methods* **160**, 335–348 (2007).
- <sup>8</sup>R. Gentner and J. Classen, "Development and evaluation of a low-cost sensor glove for assessment of human finger movements in neurophysiological settings," *J. Neurosci. Methods* **178**(1), 138–147 (2009).
- <sup>9</sup>C. Y. Park, J. Bae, and I. Moon, "Development of wireless data glove for unrestricted upper-extremity rehabilitation system," in *2009 ICCAS-SICE* (IEEE, 2009), pp. 790–793.
- <sup>10</sup>M. R. Golomb, M. Barkat-Masih, B. Rabin, M. Abdelbaky, M. Huber, and G. Burdea, "Eleven months of home virtual reality telerehabilitation—Lessons learned," in *2009 Virtual Rehabilitation International Conference* (IEEE, 2009), pp. 23–28.
- <sup>11</sup>A. Mohan, S. R. Devasahayam, J. George, and G. Tharion, "A sensorized glove and ball for monitoring hand rehabilitation therapy in stroke patients," in *Proceedings of the 2013 Texas Instruments India Educators' Conference, THIEC '13* (IEEE Computer Society, Washington, DC, USA, 2013), pp. 321–327.
- <sup>12</sup>N. Friedman, V. Chan, D. Zondervan, M. Bachman, and D. J. Reinkensmeyer, "Musicglove: Motivating and quantifying hand movement rehabilitation by using functional grips to play music," in *2011 Annual International Conference of the IEEE Engineering in Medicine and Biology Society* (IEEE, 2011), pp. 2359–2363.
- <sup>13</sup>N. Friedman, V. Chan, A. N. Reinkensmeyer, A. Beroukhim, G. J. Zambano, M. Bachman, and D. J. Reinkensmeyer, "Retraining and assessing hand movement after stroke using the musicglove: Comparison with conventional hand therapy and isometric grip training," *J. Neuroeng. Rehabil.* **11**(1), 76 (2014).
- <sup>14</sup>B. O'Flynn, J. T. Sanchez, J. Connolly, J. Condell, K. Curran, P. Gardiner, and B. Downes, "Integrated smart glove for hand motion monitoring," in *The Sixth International Conference on Sensor Device Technologies and Applications* (IARIA, 2015).
- <sup>15</sup>J. Shin, M. Kim, J. Lee, Y. Jeon, S. Kim, S. Lee, B. Seo, and Y. Choi, "Effects of virtual reality-based rehabilitation on distal upper extremity function and health-related quality of life: A single-blinded, randomized controlled trial," *J. Neuroeng. Rehabil.* **13**(1), 17 (2016).
- <sup>16</sup>G. Placidi, L. Cinque, A. Petracca, M. Polsinelli, and M. Spezialetti, "A virtual glove system for the hand rehabilitation based on two orthogonal leap motion controllers," in *Proceedings of the 6th International Conference on Pattern Recognition Applications and Methods—Volume 1* (ICPRAM, 2017), pp. 184–192.

- <sup>17</sup>See <http://www.neofect.com/en/product/rapael/> for neofect; accessed 03 August 2018.
- <sup>18</sup>See <http://www.cyberglovesystems.com/cyberglove-ii/> for cyberglove systems; accessed 04 August 2018.
- <sup>19</sup>See <http://www.5dt.com/data-gloves/> for fifth dimension technologies; accessed 03 August 2018.
- <sup>20</sup>See <http://www.dg-tech.it/vhand3/products.html> for dgtech engineering solutions; accessed 04 August 2018.
- <sup>21</sup>See <https://www.virtualmotionlabs.com/vr-gloves/vr-glove/> for virtual motion labs; accessed 03 August 2018.
- <sup>22</sup>See <https://www.virtualmotionlabs.com/vr-gloves/vmg-10/> for virtual motion labs; accessed 03 August 2018.
- <sup>23</sup>J. L. Hernandez-Rebollar, N. Kyriakopoulos, and R. W. Lindeman, "The aceleglove: A whole-hand input device for virtual reality," in *Proceedings of SIGGRAPH* (IEEE, 2002), Vol. 85, p. 259.
- <sup>24</sup>See <https://www.leapmotion.com/technology/> for leap motion; accessed 03 August 2018.
- <sup>25</sup>H. M. Schepers, D. Roetenberg, and P. H. Veltink, "Ambulatory human motion tracking by fusion of inertial and magnetic sensing with adaptive actuation," *Med. Biol. Eng. Comput.* **48**, 27–37 (2009).
- <sup>26</sup>H. G. Kortier, J. Antonsson, H. M. Schepers, F. Gustafsson, and P. H. Veltink, "Hand pose estimation by fusion of inertial and magnetic sensing aided by a permanent magnet," *IEEE Trans. Neural Syst. Rehabil. Eng.* **23**(5), 796–806 (2015).
- <sup>27</sup>E. R. Bachmann, R. B. McGhee, X. Yun, and M. J. Zyda, "Inertial and magnetic posture tracking for inserting humans into networked virtual environments," in *Proceedings of the ACM Symposium on Virtual Reality Software and Technology, VRST '01* (ACM, New York, NY, USA, 2001), pp. 9–16.
- <sup>28</sup>S. O. H. Madgwick, A. J. L. Harrison, and R. Vaidyanathan, "Estimation of IMU and MARG orientation using a gradient descent algorithm," in *2011 IEEE International Conference on Rehabilitation Robotics* (IEEE, 2011), pp. 1–7.
- <sup>29</sup>G. Wu, F. C. T. van der Helm, H. E. J. (DirkJan)Veeger, M. Makhsous, P. V. Roy, C. Anglin, J. Nagels, A. R. Karduna, K. McQuade, X. Wang, F. W. Werner, and B. Buchholz, "ISB recommendation on definitions of joint coordinate systems of various joints for the reporting of human joint motion-Part II: Shoulder, elbow, wrist and hand," *J. Biomech.* **38**, 981–992 (2005).
- <sup>30</sup>A. Godwin, M. Agnew, and J. Stevenson, "Accuracy of inertial motion sensors in static, quasistatic, and complex dynamic motion," *J. Biomech. Eng.* **131**(11), 114501–114505 (2009).
- <sup>31</sup>G. Aslan and A. Saranlı, "Characterization and calibration of mems inertial measurement units," in *2008 16th European Signal Processing Conference* (IEEE, 2008), pp. 1–5.
- <sup>32</sup>L. Ricci, D. Formica, L. Sparaci, F. R. Lasorsa, F. Taffoni, E. Tamilia, and E. Guglielmelli, "A new calibration methodology for thorax and upper limbs motion capture in children using magneto and inertial sensors," *Sensors* **14**(1), 1057–1072 (2014).
- <sup>33</sup>L. Ricci, F. Taffoni, and D. Formica, "On the orientation error of IMU: Investigating static and dynamic accuracy targeting human motion," *PLoS One* **11**(9), e0161940 (2016).
- <sup>34</sup>H. G. Kortier, V. I. Sluiter, D. Roetenberg, and P. H. Veltink, "Assessment of hand kinematics using inertial and magnetic sensors," *J. Neuroeng. Rehabil.* **11**(1), 70 (2014).
- <sup>35</sup>Y. Lai, S. Jan, and F. Hsiao, "Development of a low-cost attitude and heading reference system using a three-axis rotating platform," *Sensors* **10**, 2472–2491 (2010).